Chapter IV

Effect of Gamma rays and 90 MeV Carbon Ion Beam Irradiation on Optical, Luminescence and Electrical Properties of Polystyrene/Eu_2O_3 Polymer Nanocomposites

In this chapter, the changes in the structural and optical, electrical, luminescence properties and surface morphology of PSE due to the incorporation of filler and irradiation with gamma rays and 90 MeV carbon ions have been investigated using various techniques.

4.1 Introduction

Over the last few years, much attention is being paid to the development of flexible, compact, and lightweight technological devices. For such properties, a polymer as a host matrix is a better choice than other host matrices. It is widely used in data storage devices, packaging, and microelectronic devices, etc. [1–3]. In the present study, Polystyrene (PS) has been used as the host matrix. One of the significant advantages of polymers is that their properties can be tuned as per need by selecting an appropriate filler, its concentration and size, and preparation condition. A suitable metal is a natural choice as a filler, as it improves the chemical and physical durability of the polymer [4–8]. In addition to metal oxides, rare earth metals are fascinating materials because their optical spectra exhibit vibronic characteristics [9]. Especially, Eu^{3+} ion is more in demand than other rare earth metal ions because of electronic transitions ($^7F_0/^5D_0$, $^5D_2$ or $^5D_0/^7F_0$, $^7F_2$) of emission, absorption, and excitation, resulting in the vibronic properties [9,10].

The polymer nanocomposites' properties can be modified through various treatments such as heating, mechanical force, chemical reaction, and ion irradiation. Often these treatments cause degradation of the polymer. Out of all the procedures, irradiation is more useful because its initiation does not require catalysts, as in the initiation of chemical reactions [11,12]. Few reports are available on modifying polymers' luminescence properties after incorporating rare-earth ions [13–15]. Irradiation affects the macroscopic properties of polymer composites causing irreversible mutations. [11]. Out of all, irradiation can be one of the important methods to modify polymers' physical and chemical properties via electronic excitation and ionization processes. In this process, the energy of ions is unevenly distributed in the material. Whereas modification of matter can be achieved uniformly using gamma irradiation [16]. Polymer films have applications, such as in radiation dosimetry, if they are irradiated with high gamma doses, as explained by Ortiz-Morales et al. [17]. Therefore, a significantly larger dose range of gamma radiation has been selected for the present work. Dosimetry is used to inhibit health risks from unspecified radiation.

The preparation method of polymer composites was the same as discussed in Chapter 2 (section 2.2). These samples were irradiated with gamma rays and SHI ion beam at IUAC, New Delhi. 1wt%, 3wt%, and 5wt% Europium (III)

oxide doped polystyrene samples are labelled in this report as PSE1, PSE3, and PSE5, respectively. The effects of gamma rays and SHI radiations on structural, optical, luminescence, thermal, and electrical properties of Polystyrene/Eu_2O_3 nanocomposites have been investigated using X-ray diffraction, UV-visible spectroscopy, photoluminescence and thermoluminescence, differential scanning calorimetry, and LCR measurements, respectively [18–20].

4.2. Results and Discussion

4.2.1 XRD Analysis

Figure 4.1 illustrates the X-ray diffraction patterns of pre-and-post irradiated Europium (III) oxide doped polystyrene films. The X-ray diffraction pattern of polystyrene shows a peak centered around 2Θ = 19.76°, which suggests partial crystalline nature with a dominant amorphous nature of polystyrene. The X-ray diffraction pattern of Europium (III) oxide doped polystyrene film shows typical peaks of Europium (III) oxide at 2Θ = 16.5°, 28.5°, 29.68°, 32.04°, 40.9° and 51.86° assigned as (200), (222), (123), (400), (422) and (235) reflections, respectively. These confirm with the BCC structure of Europium (III) oxide (JCPDS card no. 86-2476).

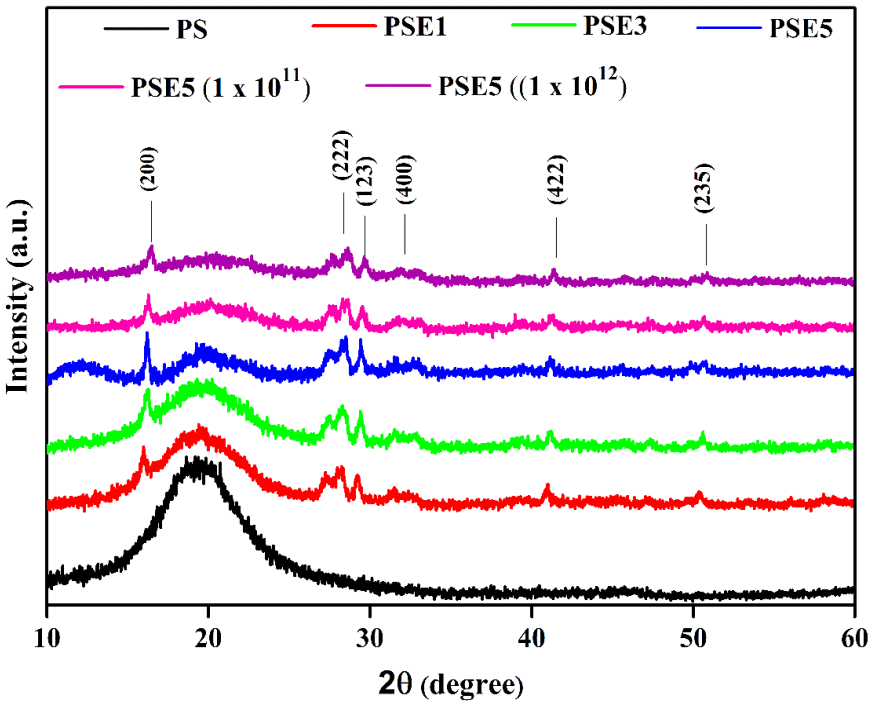

Figure 4.1 XRD spectra of pristine and irradiated polymer composites.

Scherrer's formula was used for the calculation of average crystallite size (D) of the polymer nanocomposites:

$$D = \frac{K\lambda}{\beta \cos\theta}$$

Where K (= 0.9) and λ (= 1.5416 Å) are shape factor and X-ray wavelength, respectively. β is the FWHM of the intensity peak of the filler. The average crystallite size of PSE film thus obtained and is listed in Table 4.1. The crystallite size of the polymeric film slightly increases with an increase in the filler concentration, whereas it slightly decreases with SHI radiation fluence. No change in crystallite size is observed after gamma irradiation due to the aromatic groups in polystyrene that are rarely damaged by the gamma irradiation dose used [21]. Moreover, SHI irradiation causes a large amount of energy to accumulate in the material, leading to a decrease in crystallite size. This result could be due to the splitting of the crystalline grains. A decrease in crystallite size reflects a decrease in crystallinity after SHI irradiation.

Sample	Average Crystallite Size (nm)
PSE1	14.98
PSE3	16.83
PSE5	20.46
PSE5 (1 x 10^{11})	17.54
PSE5 (1 x 10^{12})	11.06

Table 4.1 Average crystallite size of pristine and irradiated PS composites.

4.2.2 Fourier Transform Infrared Spectroscopy

Figure 4.2 depicts FTIR transmittance spectra of the polystyrene/Europium (III) oxide nanocomposites, obtained in the wavenumber range 3200-400 cm^{-1}. FTIR spectra were used to study functional groups or chemical bonds in PS and PS/Europium (III) oxide nanocomposite. The spectra of polystyrene (PS) exhibit characteristic peaks centered around 757, 906, 979, 1451, 1496, 1583, 2850 and 3000 cm^{-1}. The peak centered at 757 cm^{-1} is assigned to bending vibration of C-H in monosubstituted phenyl ring. The stretching vibrations of phenyl rings are observed at peaks centered 1451 and 1496 cm^{-1}. Peaks at 906 and 979 cm^{-1} are attributed to the C-H rocking mode. The bands observed in the range 2800-3100 cm^{-1} can be assigned to the C-H stretching vibration in the phenyl group and main

chain. In IR spectra of PS/Eu_2O_3 nanocomposites, the new weaker bands have been observed at 418 and 1704 cm^{-1}, describing stretching vibration of Eu-O bond and C=O groups, respectively [22].

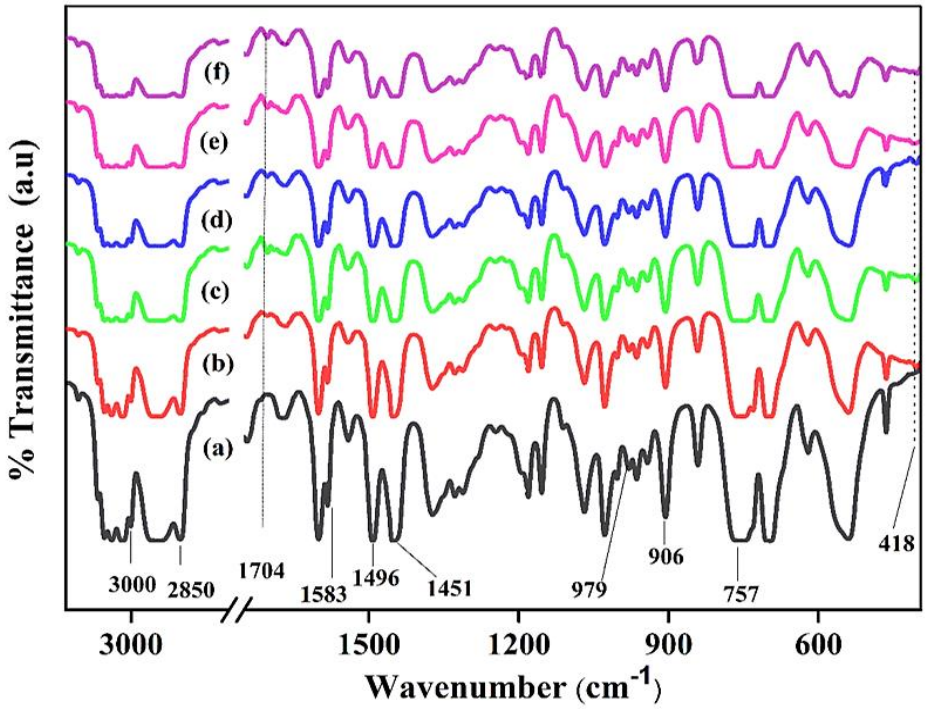

Figure 4.2 FTIR spectra of (a) PS, (b) PSE1,(c) PSE3, (d) PSE5, (e) PSE5 (1 x 10^{11}) and (f) PSE5 (1 x 10^{12}).

The intensity of all peaks decreases due to the incorporation of the filler. It could be attributed to the presence of Europium (III) oxide in polystyrene. This feature may be assigned to the interaction between the polymer matrix with the nanofiller. The profile of FTIR spectra of pristine and irradiated PS/Europium (III) oxide is the same as that of pure PS. There is no alteration in the intensity of PS/Eu_2O_3 nanocomposites' vibrational bands after gamma irradiation. The existence of the benzene ring in polystyrene is responsible for radiation stability [21].

However, the value of LET for C^{6+} ions is too high compared to the case of gamma-rays irradiation. This considerable value of LET indicates that the carbon ions can break off all linkages within a few nanometer regions around their trajectory [16,23,24]. Thus, after SHI irradiation, the intensity of all the above-described bands decreases. The reduction of peak intensity after SHI irradiation results from scissioning a few or more carbonate bonds and reducing hydrogen from the backbone of the polymer. These results point to possible enhancement of

PS/Europium (III) oxide polymer nanocomposites' optical and electrical properties after SHI irradiation.

4.2.3 UV-Visible Analysis

Figure 4.3 depicts the optical response of pristine and irradiated polymeric films. The $\pi \rightarrow \pi^*$ electronic transition in the benzene ring is responsible for the observed absorption by PS. UV absorption spectra of nanocomposites show weak intensity peaks about wavelengths 370 nm and 401 nm, suggesting the presence of Eu^{3+}. The peaks appearing at 370 nm and 401 nm can be ascribed to $^7F_0 \rightarrow {}^5D_4$ and $^7F_0 \rightarrow {}^5L_6$ transitions of Eu^{3+}, respectively [25]. The absorption edge of PS is found at 280 nm. A redshift of the absorption edge has been observed with the increase in europium (III) oxide concentration. It is a consequence of the formation of coordination bonds among Eu^{3+} ions and the carbonyl group of the polymer matrix. Moreover, irradiation causes the absorption edge to re-migrate towards a longer wavelength, which is the result of breakage as well as the formation of a few of the bonds. These results imply an alteration in the polymer films' optical bandgap after incorporating the filler and irradiation [26–28].

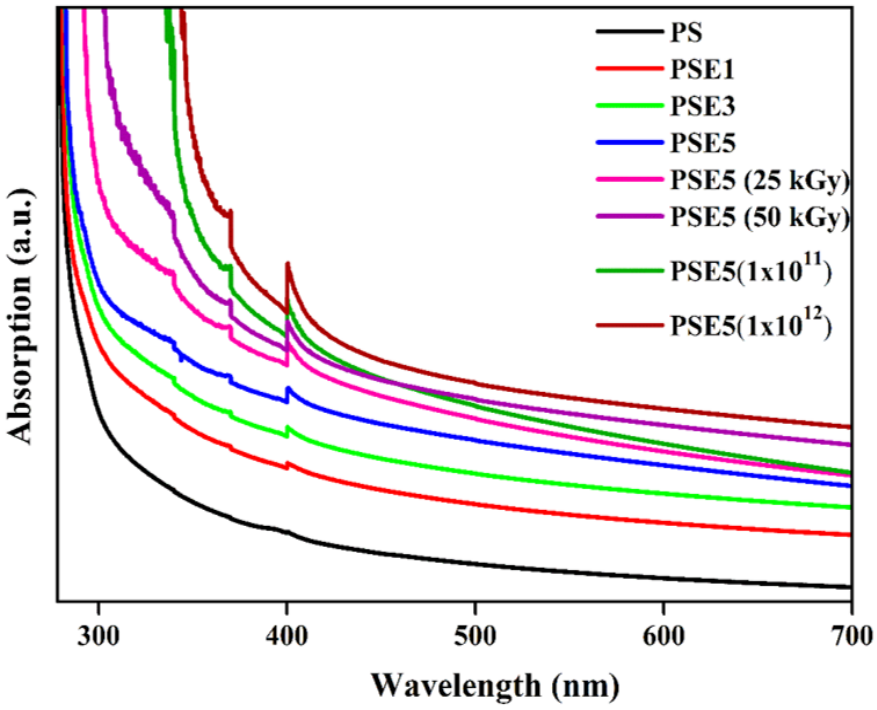

Figure 4.3 Optical response of pre and post-irradiated-films.

Sample	Bandgap (eV)	Number of carbon hexagon rings
PS	4.38	1
PSE1	4.21	1
PSE3	4.15	1
PSE5	4.08	1
PSE5 (25 kGy)	3.86	1
PSE5 (50 kGy)	3.67	1
PSE5 (1 x 10^{11})	3.47	1
PSE5 (1 x 10^{12})	3.31	2

Table 4.2 Bandgap of Polystyrene, its composites and irradiated samples.

Determination of Optical Bandgap:

The modification in the optical bandgap of polystyrene with the filler concentration and irradiation dose was computed using Tauc's equation [29]:

$$\alpha hv = B(hv - E_g)^n$$

Where n = number corresponding to the transition process in K-space. For direct optical bandgap, the value of n is 0.5. B is a constant. The quantities hv, α and E_g are photon energy, absorption coefficient and optical band gap, respectively. The direct bandgap is obtained by extrapolating the higher energy range linear nature of the $(\alpha hv)^2$ vs hv curve to give an intercept on X-axis (i.e. energy axis). The value of the optical band gap thus obtained is listed in Table 4.2. As the concentration of the filler increases, the optical band gap decreases. These results indicate the occurrence of local cross-linking inside the polymer matrix. Furthermore, the bandgap reduction is inferred to be a function of irradiation dose, which suggests an alteration of the aromatic structure to a graphite-like structure. These results also indicate chain scission of the polymer matrix. The effect of gamma irradiation on optical bandgap is less than that of SHI irradiation. This may be attributed to high structural disorder induced by SHI irradiation. This can be explained by the density of state model in noncrystalline solids suggested by Mott and Davis [30]. According to this model, the structural disorder in polymer matrices results in decreased bandgap and increased conductivity.

The number of C_6 rings (M) in the compact carbonaceous cluster was determined using the equation [31]:

$$E_g = 2\,|\beta|\,M^{-0.5}$$

Here, the parameter $|\beta|$ represents the nearest-neighbour interaction between π orbitals. The value of M (~1) remains the same for pre and gamma-irradiated PSE5, whereas that of SHI irradiated PSE5 is 2. This suggests an increased rate of dehydrogenation process in the latter case [16].

4.2.3 Photoluminescence

Photoluminescence emission spectra of Europium (III) oxide doped PS films were recorded at 247 nm excitation wavelength. Whereas the excitation spectrum was obtained at 616 nm emission wavelength at room temperature. Photoluminescence excitation and emission spectra of pristine polymer films are shown in figures 4.4 and 4.5, respectively. In the excitation spectra, the broad peak centered at 247 nm may be ascribed to charge transfer transition between the carbonyl group of the polymer matrix and Eu^{3+} ions. The emission peaks of PS (in the range of 360-410 nm) arise due to carbonyl group formation during exposure to light. The emission spectra of Eu^{3+} doped polystyrene show peaks at 595 nm, 612 nm and 617 nm, which correspond to $^5D_0 \rightarrow {}^7F_1$ and $^5D_0 \rightarrow {}^7F_2$ transitions, respectively. These f-f transitions $^5D_0 \rightarrow {}^7F_1$ and $^5D_0 \rightarrow {}^7F_2$ are associated with magnetic and electric dipole transitions, respectively. Integral intensity ratio R (i.e., the ratio of intensities of electric dipole transition and magnetic dipole transition) are used to infer the site symmetry of Eu^{3+} ions in the polymer matrix lied below one for pristine and irradiated nanocomposites [32,33]. The PL intensity of magnetic dipole transition is seen to be weaker than the PL intensity of electric dipole transition. From the value of R, Eu^{3+} ions seem to reside at non-centrosymmetric sites of the polymer matrix [34–38]. Also, electric dipole transitions are responsible for intense red emission. The intensity of characteristic peaks of Eu^{3+} ions increases with the increase in the filler's concentration, while the peak intensity corresponding to the PS is observed to decrease. This could be explained by the augmentation of charge carriers. They play a crucial role in decreasing the activation of a singlet excitation state. It implies that the number of defects increases in polystyrene due to doping of Eu_2O_3, implying alteration of the non-radiative and radiative recombination processes.

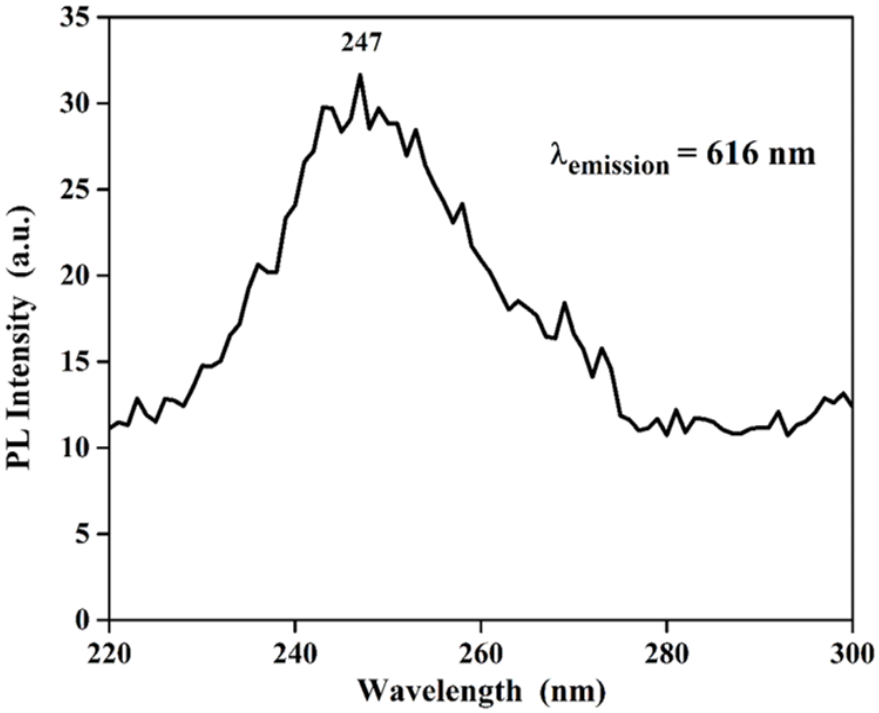

Figure 4.4 Photoluminescence excitation spectrum of PS/Eu_2O_3 nanocomposites.

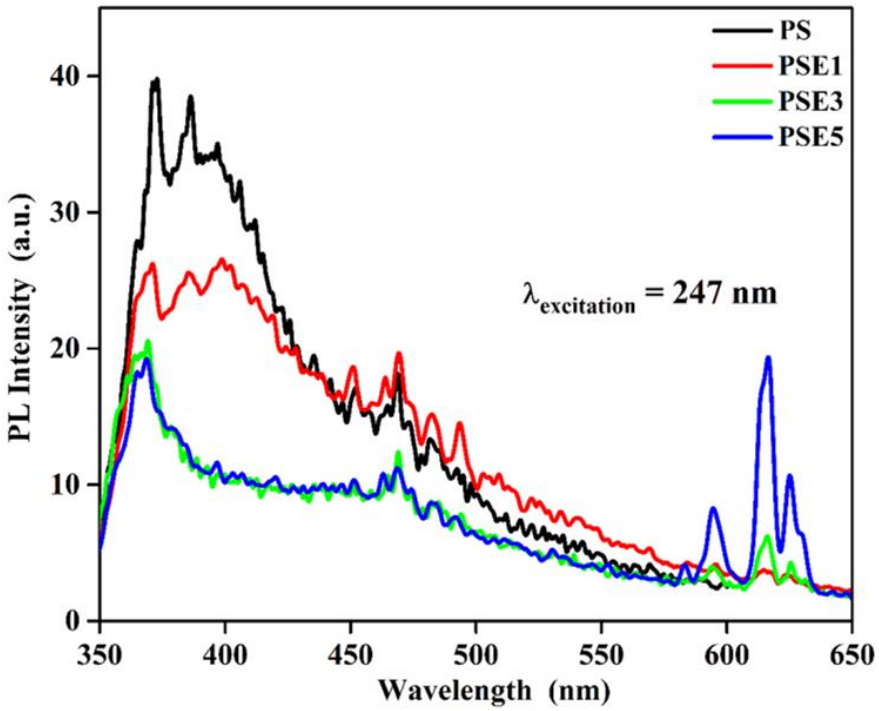

Figure 4.5 Photoluminescence emission spectra of pristine polystyrene composite films.

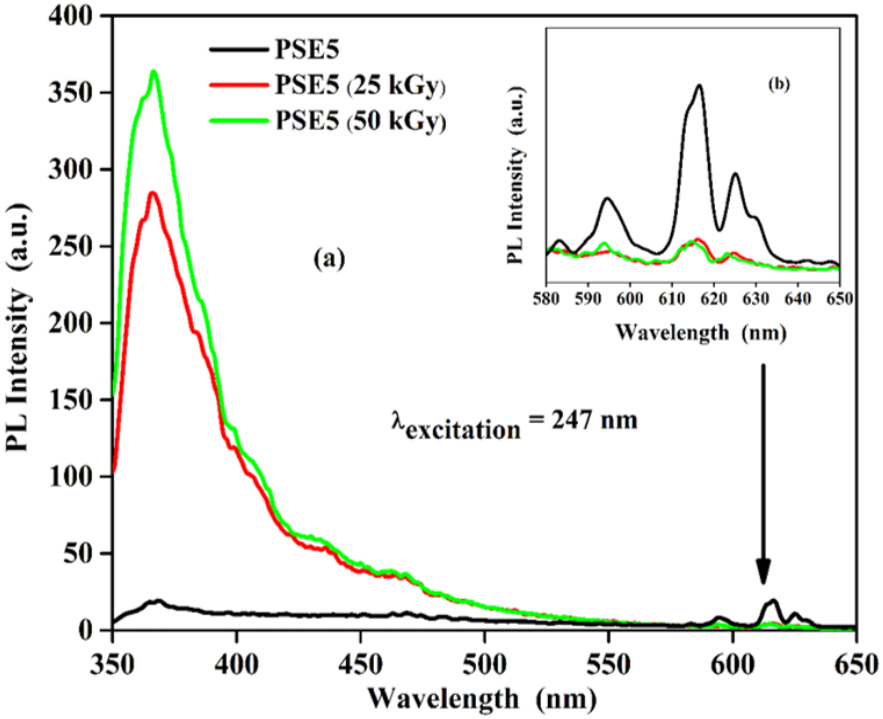

Figure 4.6 Photoluminescence emission spectra of (a) PSE5 film irradiated with gamma rays at the dose of 25 kGy and 50 kGy (b) magnified peaks in the range of 580-650 nm **.**

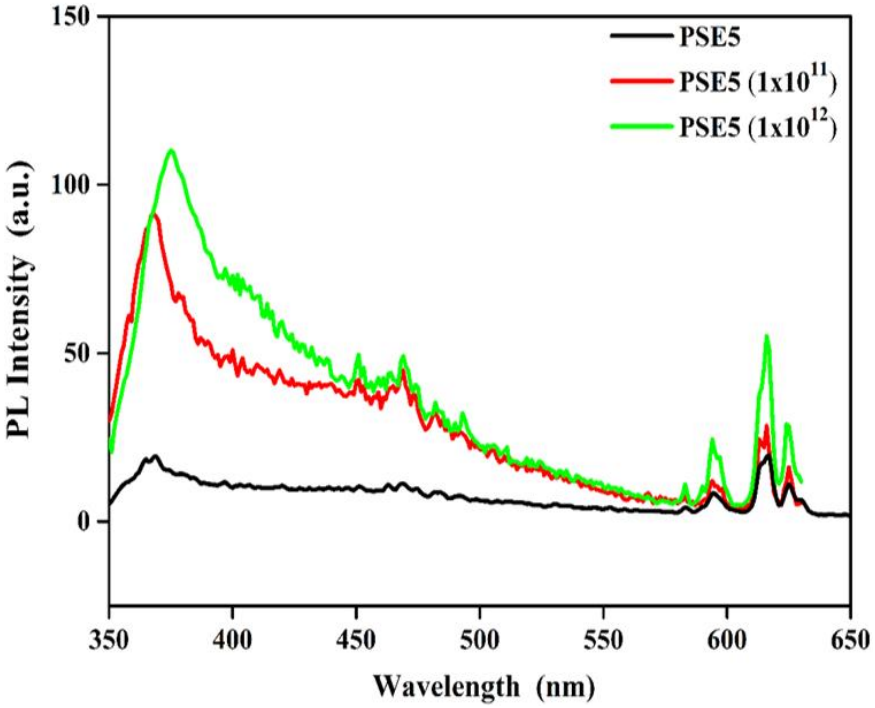

Figure 4.7 Photoluminescence emission spectra of PSE5 film irradiated with SHI at the fluence of $1x10^{11}$ and $1x\ 10^{12}$ ions/cm^2.

The change in the photoluminescence spectrum of PSE5 with gamma and SHI irradiations is shown in figures 4.6 & 4.7, respectively. Gamma irradiation

causes a decrease in the PL intensity of Eu^{3+} ions. This decrease may be attributed to the formation of defects that support the non-radiative transition and create additional paths, hence the decrease in intensity of Eu^{3+} PL emission. In contrast, the intensity of PL emission peaks of PS and Eu^{3+} ions increases after SHI irradiation. SHI irradiation produces more defects than gamma rays irradiation, which leads to an intense Eu^{3+} emission. Moreover, the irradiation may also be responsible for forming the system of conjugated bonds and carbon enriched polymer by extracting hydrogen and its transformation into a graphite-like structure that explains the systems' unusual behaviour after gamma rays irradiation.

4.2.5 Thermoluminescence

Thermoluminescence (TL) study of PS/Eu_2O_3 polymer composites includes a variation of TL output with irradiation dose. Figures 4.8 & 4.9 depict TL glow curves of PS/Eu_2O_3 polymeric films irradiated with gamma rays and SHI radiation, respectively. The TL glow curves appear when nanocomposites are heated after being exposed to the radiations. Free charge carriers arise due to irradiation; most of them are recombined within a short time. But a few of them get enough energy to survive without recombining and get trapped in localized sites or defect sites. During heating treatment, the trapped electrons can gain enough energy to get released due to the motion of macromolecules or thermal excitation or rupture of traps. These free electrons recombine with holes in the valence band via conduction band into TL maxima. The glow curve deconvolution (GCD) method was used to analyze the TL glow curves' output. Figures 4.10 & 4.11 illustrate the TL glow curve fitting of PSE5 polymer nanocomposites. This fitted glow curves exhibit complex behaviour, which indicates that the GCD method is more useful than the other methods. The GCD fitting of TL glow curves follow the general order kinetics equation given by Kitis et al. [39] as follows:

$$I(T) = I_m b^{b-1} \exp\left(\frac{E_a}{k_B T}\left(\frac{T - T_m}{T_m}\right)\right)\left[(b-1)\frac{T^2}{{T_m}^2}\left(1 - \frac{2k_B T}{E_a}\right)\exp\left(\frac{E_a}{k_B T}\left(\frac{T - T_m}{T_m}\right)\right) + 1 + (b-1)\frac{2k_B T_m}{E_a}\right]^{(b-1)}$$

where, *b*, *s*, *E* and *k* are kinetic parameters, frequency factor, activation energy and Boltzmann constant, respectively. The temperature at maximum intensity I_m is labeled as T_m. Values of *b*, *s*, T_m and *E* of GCD fitted curve are given in Table 4.3.

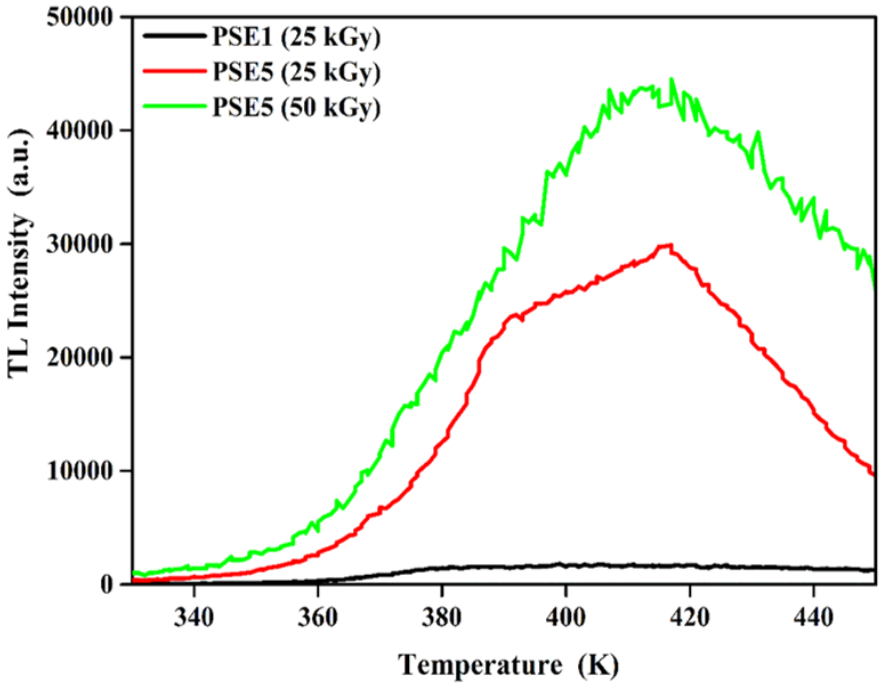

Figure 4.8 TL glow curves of gamma rays irradiated polymer nanocomposites.

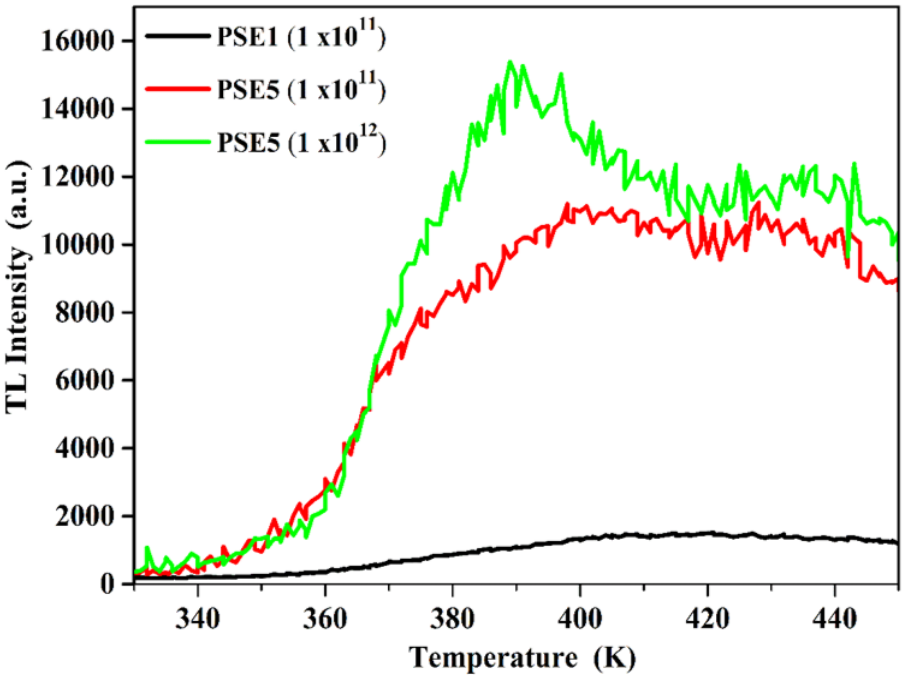

Figure 4.9 TL glow curve for 90 MeV carbon ion beam irradiated polymeric films.

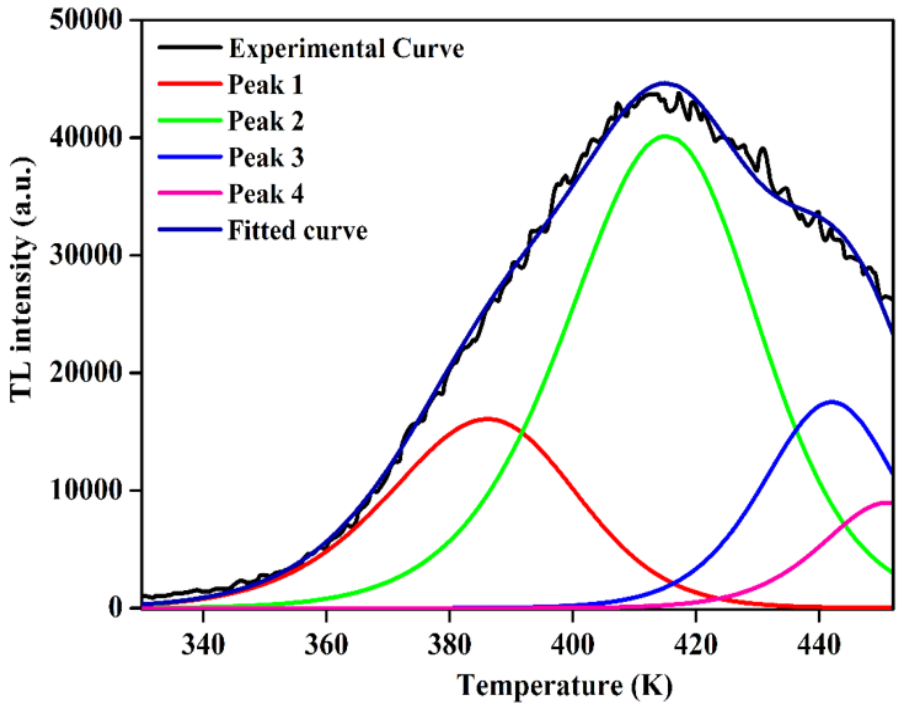

Figure 4.10 GCD fitting of TL glow curve of 50 kGy gamma rays irradiated PSE5 polymer composites.

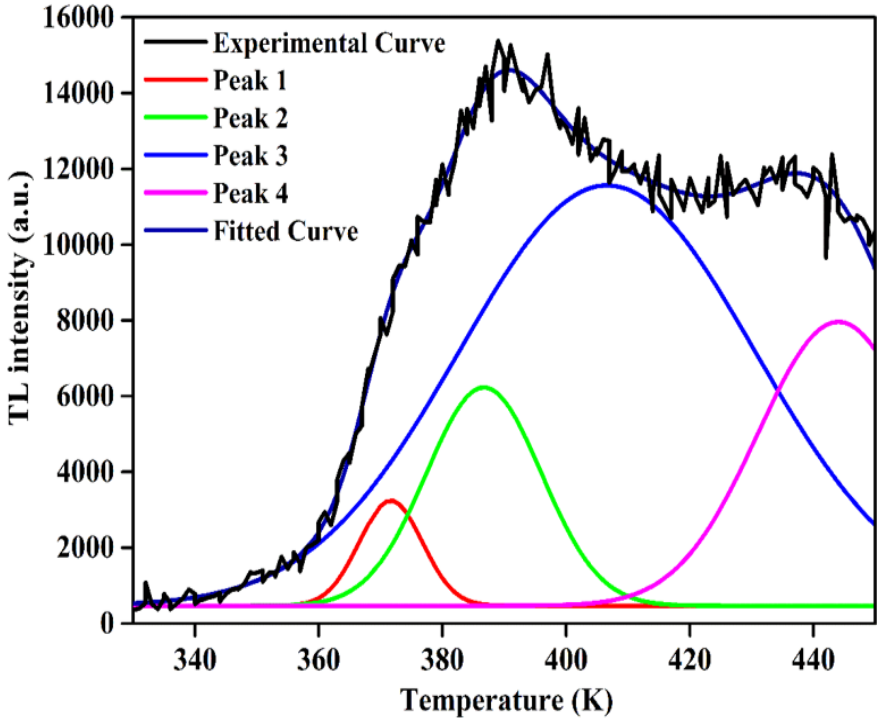

Figure 4.11 GCD fitting of TL glow curve of 90 MeV carbon ion irradiated PSE5($1x10^{12}$) polymer composites.

Samples	Fluence	Peak	T_m (K)	E (eV)	B	s (s^{-1})
PSE5 (gamma irradiated)	50 kGy	1	386	1	1.44	6.7×10^{11}
		2	415	1.17	1.54	9.4×10^{12}
		3	442	2.0	1.73	5.2×10^{21}
		4	451	2.1	1.4	2.2×10^{22}
PSE5 (SHI beam irradiated)	1×10^{12} ions/cm^2	1	371	2.89	1.671	1.87×10^{22}
		2	387	1.9	1.8	1.58×10^{17}
		3	407	0.736	1.63	1.48×10^{7}
		4	445	0.75	1.845	1.30×10^{7}

Table 4.3 Kinetic parameter and activation energy for glow, as calculated from GCD for irradiated PSE5 films.

The activation energy of all GCD fitted curves of PSE5 irradiated with gamma rays, and SHI beam is found to be in the range of 1 eV- 2.1 eV and 0.736 eV - 2.89 eV, respectively. The change in the frequency factor of PSE5 irradiated with gamma rays and SHI beam is found to be in the range 10^{11} to 10^{22} s^{-1} and 10^{7} to 10^{22} s^{-1}, respectively. The peak temperature (T_m) of TL glow curves of nanocomposite films lies between 378 K and 444 K.

The considerable variation in activation energy suggests a random distribution of traps. As regards the TL maxima, the trapped electrons are released from trapping centers due to different relaxation processes such as β, γ and δ relaxations. From the value of peak temperature, the detrapping of electrons seems to be caused by γ and β - relaxations. The γ – relaxation relates to the torsional motion of the methylene group produced in the backbone chain, while β - relaxation corresponds to the rotation of the benzene ring and/or rotational vibration of the main segments of polystyrene [40].

TL analysis of nanocomposites shows that the intensity of glow curves improves with irradiation dose. The result can infer to imply that trapping centers' growth inside the polymer matrix increases with irradiation dose [41]. These results also correlate with the results obtained from photoluminescence analysis and suggested that PSE5 can be used for dosimetry applications [42]. Figures 4.8

& 4.9 show that the TL yield of SHI irradiated PSE5 is lower than that of gamma-rays irradiated PSE5.

4.2.6 AC Electrical Properties

4.2.6.1 Dielectric Constant

`The frequency-dependent dielectric constant of pristine and irradiated polymeric films are depicted in figure 4.12. The dielectric constant of the polymer shows a decreasing tendency with increasing frequency. At low frequencies, the charge carriers in the polymeric films have a long-range drift due to a slow varying electric field, which causes the high value of dielectric constant at low frequency. The dielectric constant declines with increasing frequency and became constant above 1 kHz. This is due to the reduction in charge carrier density at the interface as a consequence of the slower response of polymeric dipoles with a significant moment of inertia to the rapid electric field variations.

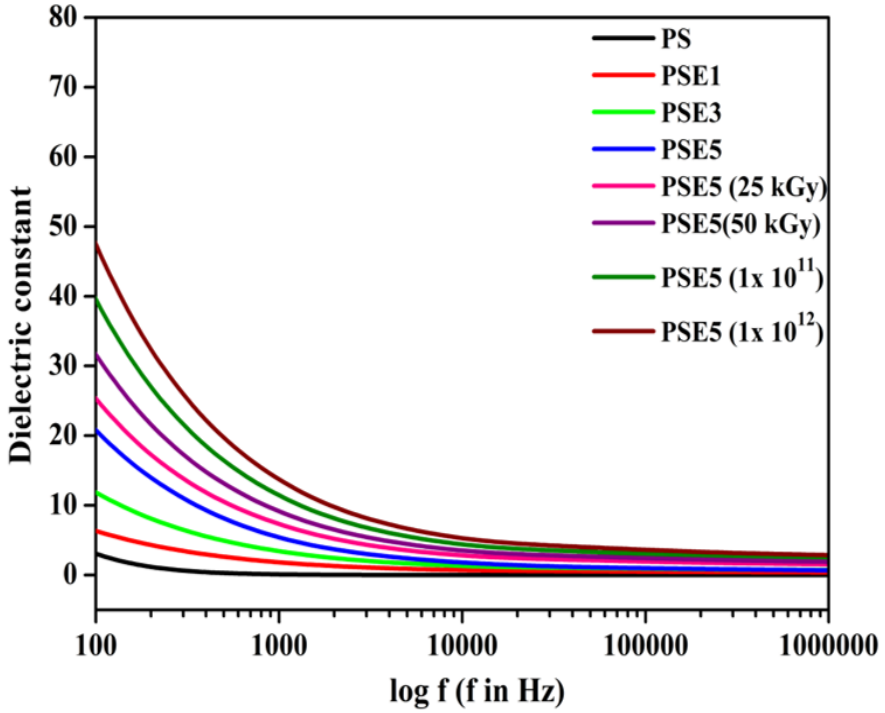

Figure 4.12 Dielectric constant vs log frequency for PS/Eu_2O_3 polymer composites.

The increase in dielectric constant with the filler concentration correlates with the interfacial polarization effect between nanoparticles and polymer matrix. The overall value of the dielectric constant increased after irradiation due to the increase in the charge carrier density and the scission of polymer chains. Also, it implies interfacial polarization of space charges. Due to the swift heavy ion

irradiation, significant degradation of the sample occurred, resulting in a more significant increase in the dielectric response than that caused by gamma-ray irradiation.

4.2.6.2 Dielectric Loss

Figure 4.13 shows the variation in dielectric loss with the frequency, the concentration of filler and radiation dose. It is found that the dielectric loss exponentially decreases with frequency. It is due to the failure of induced charges to adhere to reversing field, resulting in the reduction of ionic oscillation.

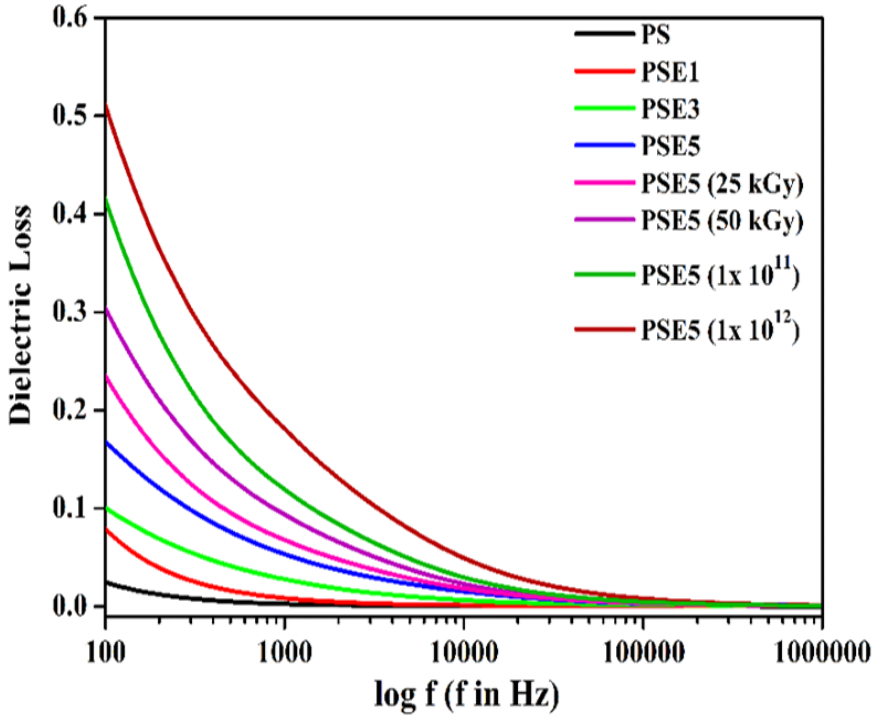

Figure 4.13 Dielectric loss vs log frequency for PS/Eu_2O_3 polymer composites.

The dielectric loss increases moderately with an increase in the concentration of filler and radiation dose. It is due to the increase in interfacial polarization. It is observed that the variation in dielectric loss of PSE5 after SHI irradiation is higher than that of gamma irradiation.

4.2.6.3 AC Electrical Conductivity

Figure 4.14 illustrates AC conductivity of pristine and irradiated samples as a function of frequency, filler level and irradiation dose. It is seen that the AC conductivity increases with filler concentration. The increase in the conductivity upon the incorporation of europium (III) oxides may be attributed to the formation of several conduction paths that cause a reduction in the width of the potential

barrier inside the bulk region with high conductivity. Therefore, more charge carriers hop through tunnelling, causing an increase in the conductivity. Usually, an increase in AC conductivity with filler level is related to the interaction process occurring in the polymer nanocomposites. After irradiation, there is an increase in the AC conductivity of polymer composites because of the promotion of filler to polymer bonding.

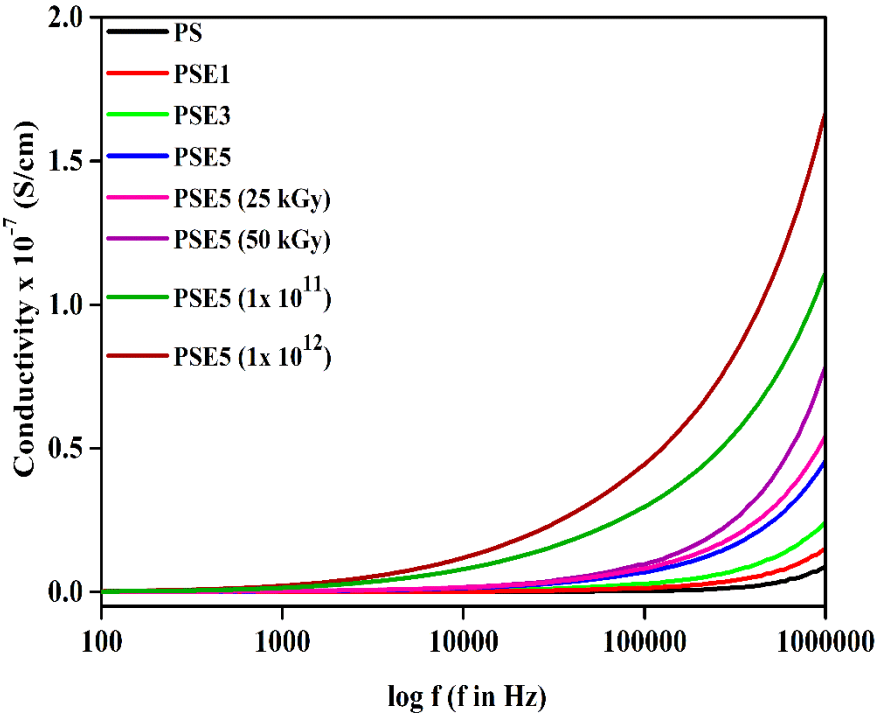

Figure 4.14 Conductivity vs log frequency for PS/Eu_2O_3 polymer composites.

It is also expected that the conversion of polymer structure to the carbon-rich network occurs due to irradiation. This carbon-rich network is supposed to be more conductive than the pristine polymer composite [16,43]. The amount of local energy deposition increases with the gamma irradiation dose and ion fluence, resulting in an increase of free electrons and impurities. Hence, the increase in electrical properties of the system upon C^{6+} ion beam irradiation is more pronounced than that of gamma irradiation due to the high value of LET of swift heavy ions [24].

4.2.7 Differential Scanning Calorimetry Analysis

DSC is an essential tool for exploring a polymeric system's thermal properties, such as glass transition temperature and melting point. Figure 4.15 shows the differential thermograms of pristine and irradiated polymer nanocomposite. The glass transition temperature (T_g) of PS is observed to be

about 335.4 K. From figure 4.15, it is found that the T_g of the polymer matrix is displaced from 335.4 K towards higher temperature due to the incorporation of filler. The shifting of glass transition temperature alludes interaction of nanoparticles with polymer matrix [44]. This result consists of results procure from XRD and FTIR analysis.

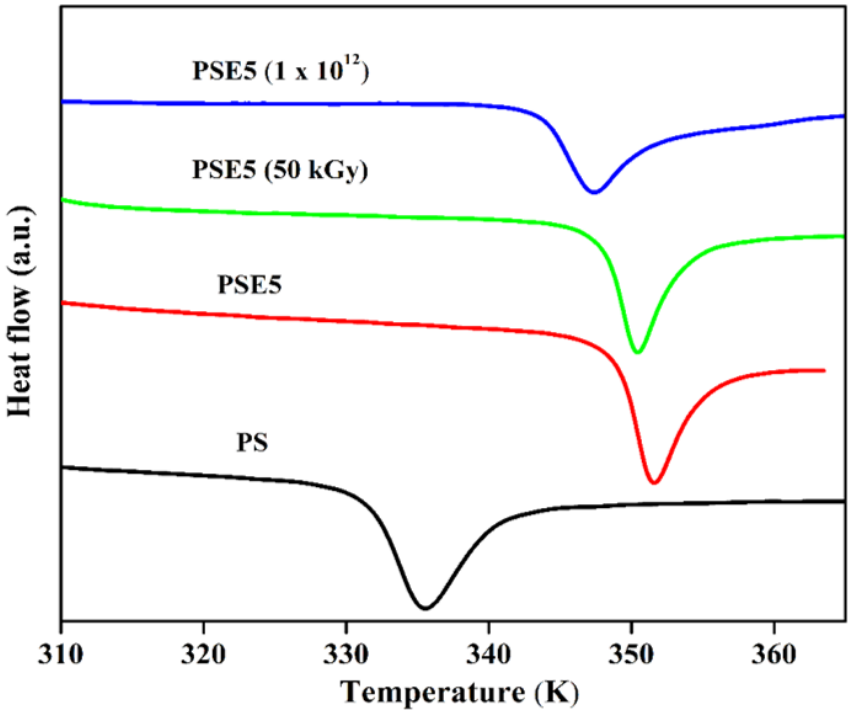

Figure 4.15 DSC thermograms of pristine and irradiated PSE films.

After both types of irradiations, the glass transition temperature of PSE5 is observed to decrease. This fact may also suggest a decrease in the degree of crystallinity. Thus an increase of macromolecular motion with irradiation dose is imperative, which might be caused due to chain scission of the polymer matrix. This result is correlated with the XRD and FTIR results.

4.2.8 Surface Morphology

Figure 4.16 depicts the three-dimensional scanned topographical images of an area of 5 x 5 μm^2 of polymeric films. These images were obtained using an atomic force microscope (AFM) used in tapping mode. The average roughness of pristine PS and PSE5 is obtained to be 9 nm and 81 nm, respectively. These results suggest that the average roughness increases due to escalated density.

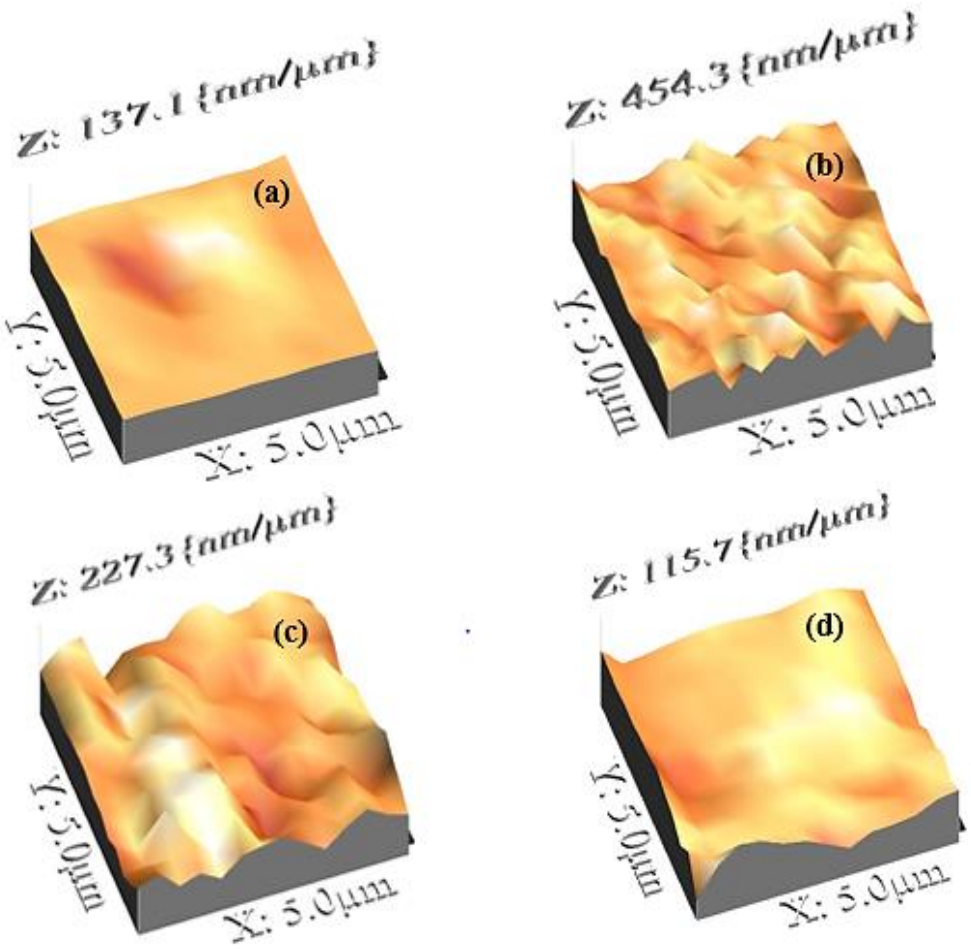

Figure 4.16 AFM of (a) PS, (b) PSE5 (c) gamma irradiated PSE5 (50 kGy) and (d) SHI irradiated PSE5 ($1x10^{12}$).

Furthermore, the value of the average roughness of gamma-irradiated PSE5 (50 kGy) and SHI irradiated PSE5 ($1x10^{12}$) is found to be 41 nm and 8 nm, respectively. It is suggested that polymeric films become smoother after both types of irradiations because of defect enhanced surface diffusion. Moreover, the changes in surface morphology of polymeric material due to swift heavy ion irradiation have been reported to be highly pronounced as compared to those due to gamma irradiation because swift heavy ions transfer more energy into polymer composite than gamma irradiation dose [16].

4.2.9 Conclusion

Irradiation causes significant changes in optical, luminescence and electrical properties of PS/Eu_2O_3 polymer nanocomposites. This considers that polymer composites are changed into hydrogen depleted carbon networks due to both kinds of irradiations. XRD analysis shows a reduction in average crystallite size after SHI irradiation, which is due to the scission of the polymer chain. The

bandgap of polymer composites decreases upon the incorporation of the filler and irradiation doses. Dielectric response significantly increases with irradiation dose as a result of the physicochemical change. The PS/Eu_2O_3 polymer composites emit red light under the excitation wavelength of 247 nm. PSE5 (50 kGy) and PSE ($1x10^{12}$) exhibit maximum TL intensity, about 43878 and 14000 units, respectively, which are good TL outputs. These observed TL outputs imply the good potential of PS/Eu_2O_3 polymer nanocomposites in dosimetry applications. Thus, improvement in the optical and electrical properties of PS/Eu_2O_3 polymer composites due to SHI irradiation is more significant than that due to gamma irradiation.

References:

[1] S. Hajati, V. Zaporojtchenko, F. Faupel, S. Tougaard, Characterization of Au nano-cluster formation on and diffusion in polystyrene using XPS peak shape analysis, Surf. Sci. 601 (2007) 3261–3267. https://doi.org/10.1016/j.susc.2007.06.001.

[2] J. Deris, S. Hajati, Reflection electron energy loss spectroscopy as efficient technique for the determination of optical properties of polystyrene intermixed with gold nanoparticles, Appl. Surf. Sci. 392 (2017) 697–700. https://doi.org/10.1016/j.apsusc.2016.09.021.

[3] S. Shah, A. Qureshi, N. L. Singh, K. P. Singh, D. K. Avasthi, Dielectric response of proton irradiated polymer composite films, Radiat. Meas. 43 (2008) 2006–2009. https://doi.org/10.1016/j.radmeas.2008.04.038.

[4] H. Xie, Z. Tang, Z. Li, Y. He, Y. Liu, H. Wang, PVDF-HFP composite polymer electrolyte with excellent electrochemical properties for Li-ion batteries, J. Solid State Electrochem. 12 (2008) 1497–1502. https://doi.org/10.1007/s10008-008-0511-9.

[5] S. Agnihotry, S. Ahmad, D. Gupta, S. Ahmad, Composite gel electrolytes based on poly(methylmethacrylate) and hydrophilic fumed silica, Electrochim. Acta. 49 (2004) 2343–2349. https://doi.org/10.1016/j.electacta.2004.01.015.

[6] S. K. Das, S. S. Mandal, A. J. Bhattacharyya, Ionic conductivity, mechanical strength and Li-ion battery performance of mono-functional and bi-functional (“Janus”) “soggy sand” electrolytes, Energy Environ. Sci. 4 (2011) 1391. https://doi.org/10.1039/c0ee00566e.

[7] G. Vijayakumar, S. N. Karthick, A. R. Sathiya Priya, S. Ramalingam, A. Subramania, Effect of nanoscale CeO_2 on PVDF-HFP-based nanocomposite porous polymer electrolytes for Li-ion batteries, J. Solid State Electrochem. 12 (2008) 1135–1141. https://doi.org/10.1007/s10008-007-0460-8.

[8] X. Huang, X. Ma, R. Wang, L. Zhang, Z. Deng, Combined effect of surface-charged latex nanoparticle AHPS and Al_2O_3 nano-fillers on electrochemical performance of the anionic gel polymer electrolytes PVA/P (MA-co-AHPS), Solid State Ionics. 267 (2014) 54–60.

https://doi.org/10.1016/j.ssi.2014.08.012.

[9] K. Annapurna, M. Das, P. Kundu, R. N. Dwivedi, S. Buddhudu, Spectral properties of Eu^{3+}: $ZnO–B_2O_3–SiO_2$ glasses, J. Mol. Struct. 741 (2005) 53–60. https://doi.org/10.1016/j.molstruc.2005.01.062.

[10] L. Mariscal-Becerra, S. Carmona-Téllez, G. V. Arredondo-Martínez, S. Salas-Mariscal, J. Hernández-Sánchez, H. Murrieta S, C. Falcony, Yttrium-europium oxide doped zinc phosphate glasses, a luminescence study, J. Non. Cryst. Solids. 471 (2017) 268–273. https://doi.org/10.1016/j.jnoncrysol.2017.06.003.

[11] A. Bhattacharya, Radiation and industrial polymers, Prog. Polym. Sci. 25 (2000) 371–401. https://doi.org/10.1016/S0079-6700(00)00009-5.

[12] P. L. Forster, D. F. Parra, J. Kai, H. F. Brito, A. B. Lugao, Influence of gamma irradiation on photoluminescence properties of polycarbonate films doped with Eu^{3+}-β-diketonate complex, Radiat. Phys. Chem. 84 (2013) 47–50. https://doi.org/10.1016/j.radphyschem.2012.06.046.

[13] B. Gao, L. Zhang, Y. Li, Effect of substituent groups with two types on benzene ring on photoluminescence property of complexes of benzoic acid—Functionalized polystyrene with Eu(III) Ion, J. Photochem. Photobiol. A Chem. 324 (2016) 23–32. https://doi.org/10.1016/j.jphotochem.2016.02.013.

[14] J. Desbiens, B. Bergeron, M. Patry, A. M. Ritcey, Polystyrene nanoparticles doped with a luminescent europium complex, J. Colloid Interface Sci. 376 (2012) 12–19. https://doi.org/10.1016/j.jcis.2012.02.020.

[15] M. Tsvirko, E. Mandowska, M. Biernacka, S. Tkaczyk, A. Mandowski, Luminescence properties of chitosan doped with europium complex, J. Lumin. 143 (2013) 128–131.

[16] A. A. El-Saftawy, A. M. Abdel Reheem, S. A. Kandil, S .A. Abd El Aal, S. Salama, Comparative studies on PADC polymeric detector treated by gamma radiation and Ar ion beam, Appl. Surf. Sci. 371 (2016) 596–606. https://doi.org/10.1016/j.apsusc.2016.03.044.

[17] A. Ortiz-morales, J. Ortiz-lopez, E. Cruz-zaragoza, R. Gómez-aguilar, Thermoluminescence and photoluminescence analyses of MEH-PPV , MDMO-PPV and RU (bpy $)_3$ gamma-irradiated polymer thin films, Appl. Rad. Iso. 102 (2015) 55–62.

[18] S. Bhavsar, G. B. Patel, N. L. Singh, Effect of γ - irradiation on optical properties of Eu_2O_3 - doped polystyrene polymer films, Luminescence. 33 (2018) 1243-1248. https://doi.org/10.1002/bio.3541.

[19] S. Bhavsar, N. L. Singh, B. Singh, Effect of γ-irradiation on thermal and thermoluminescence properties of polystyrene/europium (III) oxide composite film, Luminescence. 35 (2019) 412-417. 10.1002/bio.3742.

[20] S. Bhavsar, G. B. Patel, N. L. Singh, D. Singh, F. Singh, Effect of 90 MeV Carbon ions on Optical, Luminescence and Electrical properties of PS/Eu_2O_3 Polymer Nanocomposite. (To be Communicate)

[21] R. Mishra, S. P. Tripathy, D. Sinha, K. K. Dwivedi, S. Ghosh, D. T. Khathing, M. Müller, D. Fink, W. H. Chung, Optical and electrical properties of some electron and proton irradiated polymers, Nucl. Instruments Methods Phys. Res. Sect. B Beam Interact. with Mater. Atoms. 168 (2000) 59–64. https://doi.org/10.1016/S0168-583X(99)00829-0.

[22] E. M. Abdelrazek, Spectroscopic studies on the effect of doping with $CoBr_2$ and $MgCl_2$ on some physical properties of polyvinylalcohol films, Phys. B Condens. Matter. 403 (2008) 2137–2142. https://doi.org/10.1016/j.physb.2007.11.029.

[23] K. S. Mann, A. Rani, M. S. Heer, Shielding behaviors of some polymer and plastic materials for gamma-rays, Radiat. Phys. Chem. 106 (2015) 247–254. https://doi.org/10.1016/j.radphyschem.2014.08.005.

[24] E. Lee, G. Rao, L. Mansur, LET effect on cross-linking and scission mechanisms of PMMA during irradiation, Radiat. Phys. Chem. 55 (1999) 293–305. https://doi.org/10.1016/S0969-806X(99)00184-X.

[25] S. Rada, A. Dehelean, E. Culea, FTIR and UV–VIS spectroscopy investigations on the structure of the europium–lead–tellurate glasses, J. Non. Cryst. Solids. 357 (2011) 3070–3073. https://doi.org/10.1016/j.jnoncrysol.2011.04.013.

[26] A. Qureshi, A. Mergen, B. Aktaş, Dielectric and magnetic properties of YIG/PMMA nanocomposites, J. Phys. Conf. Ser. 153 (2009). https://doi.org/10.1088/1742-6596/153/1/012061.

[27] G. B. Patel, S. Bhavsar, N. L. Singh, F. Singh, P. K. Kulriya, SHI induced modification in structural, optical, dielectric and thermal properties of poly ethylene oxide films, Nucl. Instruments Methods Phys. Res. Sect. B Beam

Interact. with Mater. Atoms. 379 (2016) 156–161. https://doi.org/10.1016/j.nimb.2016.04.018.

[28] N. L. Singh, A. Qureshi, N. Shah, A. K. Rakshit, S. Mukherjee, A. Tripathi, D. K. Avasthi, Surface modification of polyethylene terephthalate by plasma treatment, Radiat. Meas. 40 (2005) 746–749. https://doi.org/10.1016/j.radmeas.2005.01.014.

[29] J. Tauc, R. Grigorovici, A. Vancu, Optical Properties and Electronic Structure of Amorphous Germanium, Phys. Status Solidi. 15 (1966) 627–637. https://doi.org/10.1002/pssb.19660150224.

[30] N. F. Mott, E. A. Davis, Electronic Processes in Non Crystalline Materials, Clarendon Press, Oxford, 1979.

[31] J. Robertson, E. P. O'Reilly, Electronic and atomic structure of amorphous carbon, Phys. Rev. B. 35 (1987) 2946–2957. https://doi.org/10.1103/PhysRevB.35.2946.

[32] M. Janulevicius, P. Marmokas, M. Misevicius, J. Grigorjevaite, L. Mikoliunaite, S. Sakirzanovas, A. Katelnikovas, Luminescence and luminescence quenching of highly efficient $Y_2Mo_4O_{15}:Eu^{3+}$ phosphors and ceramics, Sci. Rep. 6 (2016) 26098. https://doi.org/10.1038/srep26098.

[33] K. Suresh, K. V. R. Murthy, C. Atchyutha Rao, N. V. Poornachandra Rao, B. Subba Rao, Synthesis and characterization of nano Sr_2CeO_4 doped with Eu and Gd phosphor, J. Lumin. 133 (2013) 96–101. https://doi.org/10.1016/j.jlumin.2011.12.045.

[34] P. Ptacek, H. Schäfer, K. Kömpe, M. Haase, Crystal Phase Control of Luminescing α-$NaGdF_4:Eu^{3+}$and β-$NaGdF_4:Eu^{3+}$ Nanocrystals, Adv. Funct. Mater. 17 (2007) 3843–3848. https://doi.org/10.1002/adfm.200600974.

[35] F. M. Emen, R. Altinkaya, Luminescence and thermoluminescence properties of $Sr_3WO_6:Eu^{3+}$ phosphor, J. Lumin. 134 (2013) 618–621. https://doi.org/10.1016/j.jlumin.2012.07.020.

[36] K. V. Dabre, K. Park, S. J. Dhoble, Synthesis and photoluminescence properties of microcrystalline $Sr_2ZnWO_6:RE^{3+}$ (RE = Eu, Dy, Sm and Pr) phosphors, J. Alloys Compd. 617 (2014) 129–134. https://doi.org/10.1016/j.jallcom.2014.07.205.

[37] X. Zhao, Y. Ding, Z. Li, T. Yu, Z. Zou, An efficient charge compensated red phosphor $Sr_3WO_6: K^+, Eu^{3+}$ – For white LEDs, J. Alloys Compd. 553

(2013) 221–224. https://doi.org/10.1016/j.jallcom.2012.10.180.

[38] V. Vishwnath, M. Srinivas, N. P. Patel, D. Modi, Synthesis and Photoluminescence Studies of Eu (III), Er (III) Doped Strontium Gadolinium Tantalum Oxide, J. Fluoresc. (2016) 277–282. https://doi.org/10.1007/s10895-015-1711-1.

[39] G. Kitis, J. M. Gomez-Ros, J. W. N. Tuyn, Thermoluminescence glow-curve deconvolution functions for first, second and general orders of kinetics, J. Phys. D. Appl. Phys. 31 (1998) 2636–2641. https://doi.org/10.1088/0022-3727/31/19/037.

[40] E. Dobruchowska, L. Okrasa, I. Glowacki, J. Ulanski, G. Boiteux, The 'wet dog' effect in polymers as seen by thermoluminescence, Polym. 45 (2004) 6027–6035. https://doi.org/10.1016/j.polymer.2004.06.019.

[41] S. Som, A. Choubey, S. K. Sharma, Luminescence studies of rare earth doped yttrium gadolinium mixed oxide phosphor, Phys. B Condens. 407 (2012) 3515–3519.

[42] N. A. Kazakis, N. C. Tsirliganis, G. Kitis, Preliminary thermoluminescence investigation of commercial pharmaceutical glass containers towards the sterilization dosimetry of liquid drugs, Appl. Radiat. Isot. 105 (2015) 130–138. https://doi.org/10.1016/j.apradiso.2015.08.005.

[43] G. B. Patel, N. L. Singh, F. Singh, Modification of chitosan-based biodegradable polymer by irradiation with MeV ions for electrolyte applications, Mater. Sci. Eng. B Solid-State Mater. Adv. Technol. 225 (2017) 150–159. https://doi.org/10.1016/j.mseb.2017.08.023.

[44] V. V. Vodnik, D. K. Božanić, E. Džunuzović, J. Vuković, J. M. Nedeljković, Thermal and optical properties of silver–poly(methylmethacrylate) nanocomposites prepared by in-situ radical polymerization, Eur. Polym. J. 46 (2010) 137–144. https://doi.org/10.1016/j.eurpolymj.2009.10.022.